Transactions on Engineering Sciences vol 5, © 1994 WIT Press, www.witpress.com, ISSN 1743-3533

Smolder spread through thin horizontal fuel layers

C. Di Blasi

Dipartimento di Ingegneria Chimica,
Universitá degli Studi di Napoli Federico II,
Piazzale V. Tecchio, 80125 Napoli, Italy

ABSTRACT

Two-dimensional smoldering combustion of a thin layer of cellulosic particles, in quiescent air, is numerically simulated. The mathematical model describes pressure and velocity variations through the Darcy law. Mass and energy balance equations are used to describe convective and diffusive transport of chemical species and convective, radiative and conductive heat transfer. In conjuction with transport phenomena, chemical processes are also taken into account to describe endothermic pyrolytic and exothermic oxidative degradation of the solid to volatiles and char and further exothermic oxidation of char. The solution is computed numerically through a finite difference formulation of the model equations, based on the hybrid scheme. The splitting of the operators allows the solution to be computed into three steps, the first dealing with chemistry and the remaining two with physics. The structure of the leading edge of the smoldering wave is dominated by oxygen diffusion from the surrounding environment. However, as heat losses from the bottom surface increase, the length of the smolder wave is successively reduced and quenching of some partially charred solid occurs.

INTRODUCTION

Noticeable progress has been made in the last 50 years towards the understanding of heat and momentum transport through porous media. Studies have been motivated by direct technological applications which include [1] pollutant dispersion across the soil, heat exchanger and chemical reactor design and optimization, drying processes and insulation of buildings and pipes. In this case, cellulosic materials (newsprint) are widely used for their efficacy and low cost. Further to transport phenomena, these highly permeable materials can allow smoldering combustion. Smoldering is essentially a non-flaming, exothermic, reacting surface propagating through the porous solid. It is particularly important in the fire safety science because it is associated with the emission of toxic gases (mainly carbon monoxide) and it is often the first step of fire initiation. The determination of the controlling mechanisms is thus of great importance for fire prevention and control.

As appears from experimental observation [2,3], the reaction zone is multi-dimensional and is characterized by different stages. The cellulosic material undergoes pyrolytic and oxidative degradation with the formation

of volatile matter and solid char which, in turn, can be oxidated. Mathematical models of smoldering combustion are however based on one-dimensional formulations [4,5] which cannot describe the multi-dimensional character of the reaction front or, if formulated for two-dimensional configurations [6], use a one-step global reaction for the description of chemical processes. The model presented in this study is more advanced in that it accounts for both pyrolysis and oxidation of fuel and oxidation of char and two-dimensional structure of the smoldering front.

COMPUTER MODEL

Chemical kinetics are described as [7]:

$$FUEL \xrightarrow{K_1} \nu_{C1} CHAR + (1 - \nu_{C1}) GAS \qquad (c1)$$

$$FUEL + \nu_{O1} O2 \xrightarrow{K_2} \nu_{C2} CHAR + (1 + \nu_{O1} - \nu_{C2}) GAS \qquad (c2)$$

$$CHAR + \nu_{O2} O2 \xrightarrow{K_3} \nu_A ASH + (1 + \nu_{O2} - \nu_A) GAS \qquad (c3)$$

The problem simulated is that of smoldering combustion propagating through an isotropic bed of cellulosic particles, in a quiescent environment, according to the schematic reported in Fig.1. Local thermal equilibrium between the solid matrix and the gases is assumed. Solid properties vary linearly from the initial solid values to the char-ash values, on dependence of the solid density. Gas and solid volumes also vary during the smoldering process, though no variation in the total volume is taken into account. Radiation heat transfer is described through an effective contribution in the thermal conductivity: $k_{rad} = 16\sigma l_r T^3/3$ where the radiation path length, l_r, is again a linear function of the solid density. The mathematical model consists of the balance equations for solid phase species (eqns. (1-3), cellulosic insulation, char and ash), gas phase species (eqns. (4) (oxygen) and (5) (total continuity)), energy (eqn.(6)), momentum (eqns.(7-8)), the state equation (eqn.(9)) and the solid volume variation equation (eqn.(10)):

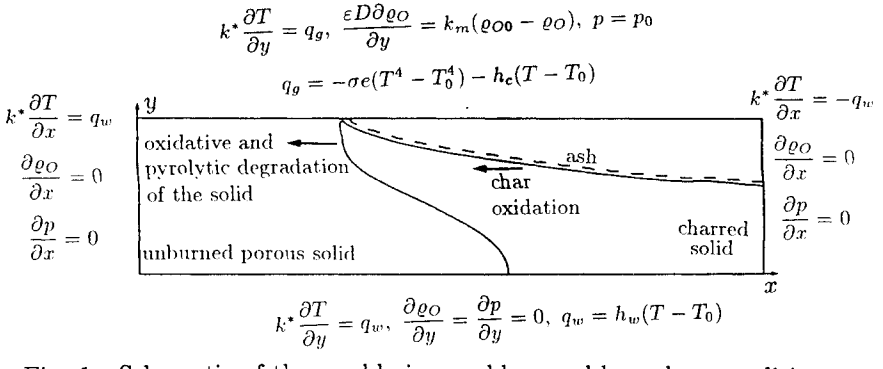

Fig. 1 - Schematic of the smoldering problem and boundary conditions.

$$\frac{\partial \rho_F}{\partial t} = -r_1 - r_2, \quad \frac{\partial \rho_C}{\partial t} = \nu_{C1} r_1 + \nu_{C2} r_2 - r_3, \quad \frac{\partial \rho_A}{\partial t} = \nu_A r_3, \qquad (1-3)$$

$$\frac{\partial(\varepsilon \varrho_O)}{\partial t} + \frac{\partial(\varrho_O u)}{\partial x} + \frac{\partial(\varrho_O v)}{\partial y} = \Omega_O + \frac{\partial}{\partial x}\left(\varrho_g D^* \frac{\partial Y_O}{\partial x}\right) + \frac{\partial}{\partial y}\left(\varrho_g^* D \frac{\partial Y_O}{\partial y}\right), \quad (4)$$

$$\frac{\partial(\varepsilon \varrho_g)}{\partial t} + \frac{\partial(\varrho_g u)}{\partial x} + \frac{\partial(\varrho_g v)}{\partial y} = \Omega_g, \qquad (5)$$

$$\frac{\partial}{\partial t}(\varrho_F h_F + \varrho_C h_C + \varrho_A h_A + \varepsilon \varrho_g h_g) + \frac{\partial}{\partial x}(\varrho_g h_g u) + \frac{\partial}{\partial y}(\varrho_g h_g v) =$$

$$\frac{\partial}{\partial x}\left(k^* \frac{\partial T}{\partial x}\right) + \frac{\partial}{\partial y}\left(k^* \frac{\partial T}{\partial y}\right) + \sum_{k=1,3} r_k \Delta h_k, \qquad (6)$$

$$u = -\frac{K}{\mu}\frac{\partial p}{\partial x}, \quad v = -\frac{K}{\mu}\left(\frac{\partial p}{\partial y} + \varrho_g g\right), \qquad (7-8)$$

$$p = \frac{\varrho_g R T}{W_g}, \quad \frac{V_s}{V_{s0}} = \frac{(\varrho_F + \varrho_C + \varrho_A)}{\varrho_{F0}}, \qquad (9-10)$$

where $r_1 = A_1 exp(-E_1/RT)\varrho_F^{nF1}$, $r_2 = A_2 exp(-E_2/RT)\varrho_F^{nF2}\varrho_O^{nO1}$, $r_3 = A_3 exp(-E_3/RT)\varrho_C^{nC1}\varrho_O^{nO2}$, $\Omega_g = (1-\nu_{C1})r_1 + (1+\nu_{O1}-\nu_{C2})r_2 + (1+\nu_{O2}-\nu_A)r_3$, $\Omega_O = -\nu_{O1}r_2 - \nu_{O2}r_3$, $\varrho_F = M_F/V$, $\varrho_C = M_C/V$, $\varrho_O = M_O/V_g$, $\varrho_g = M_g/V_g$, $V_g = (V - V_s)$, $\varepsilon = (V - V_s)/V$, $h_F = c_F(T - T_0)$, $h_C = c_C(T - T_0)$, $h_g = c_g(T - T_0)$, $h_A = c_A(T - T_0)$, $k^* = \eta k_F + (1-\eta)k_C + \varepsilon k_g + k_{rad}$, $K = \eta K_F + (1-\eta)K_C$, $D^* = \varepsilon D$, $\eta = (\varrho_F + \varrho_C + \varrho_A)/\varrho_{F0}$. The symbols have the following meaning: A pre-exponential factor, E activation energy, n order of reaction, ϱ density, ν stoichiometric coeffcient, ε porosity, u and v velocity components, Y mass fraction, T temperature, c thermal capacity, k thermal conductivity, D diffusion coefficient, M mass, V volume, Δh heat of reaction, K permeability, μ viscosity, p pressure, W molecular weight, σ Stefan-Boltzmann constant. Subscripts indicate: F fuel, C char, A ash, O oxygen, g total gas, 0 initial or reference conditions.

The bed is initially assumed at ambient conditions ($T_0 = 300K, Y_{O0} = 0.23$) and the ignition source (at temperatures of about $600K$) is active for a fixed time to cause ignition (about $120s$). Boundary conditions for the smoldering problem (eqns. (1-10)) are reported in Fig.1.

The numerical solution of eqns.(1-10) with initial and boundary conditions, over each time step Δt, is obtained by solving first the model describing chemical processes and then, using the last available values as the starting ones, the model describing only physical processes. The splitting of the operators is motivated by the different characteristic times associated with the processes of interest. More precisely, the solution is computed by

three steps. The first deals with a system of ordinary differential and algebraic equations, describing the variations in species densities, temperature and porosity caused by chemical reactions and the associated heat release:

$$\frac{\partial \rho_F}{\partial t} = -r_1 - r_2, \quad \frac{\partial \rho_C}{\partial t} = \nu_{C1} r_1 + \nu_{C2} r_2 - r_3, \quad \frac{\partial \rho_A}{\partial t} = \nu_A r_3, \qquad (1-3)$$

$$\varepsilon \frac{\partial \varrho_O}{\partial t} + \varrho_O \frac{\partial \varepsilon}{\partial t} = \Omega_O, \qquad (11)$$

$$(c_F \varrho_F + c_C \varrho_C + c_A \varrho_A + c_g \varepsilon \varrho_g) \frac{\partial T}{\partial t} =$$

$$-\left(c_F \frac{\partial \rho_F}{\partial t} + c_C \frac{\partial \rho_C}{\partial t} + c_A \frac{\partial \rho_A}{\partial t} + c_g \frac{\partial (\varepsilon \rho_g)}{\partial t}\right)(T - T_0) + \sum_{k=1,3} r_k \Delta h_k, \qquad (12)$$

$$\varepsilon = [V - V_{s0} \frac{(\varrho_F + \varrho_C + \varrho_A)}{\varrho_{F0}}]/V, \qquad (13)$$

where eqn.(13) is obtained from the solid volume evolution equation (10) and the definition of medium porosity.

The second step describes oxygen concentration and heat transport:

$$\varepsilon \frac{\partial \varrho_O}{\partial t} + \frac{\partial (\varrho_O u)}{\partial x} + \frac{\partial (\varrho_O v)}{\partial y} = \frac{\partial}{\partial x}\left(\varrho_g D^* \frac{\partial Y_O}{\partial x}\right) + \frac{\partial}{\partial y}\left(\varrho_g^* D \frac{\partial Y_O}{\partial y}\right), \qquad (14)$$

$$(c_F \varrho_F + c_C \varrho_C + c_A \varrho_A + \varepsilon c_g \varrho_g) \frac{\partial T}{\partial t} + c_g \frac{\partial}{\partial x}(\varrho_g (T - T_0) u) +$$

$$c_g \frac{\partial}{\partial y}(\varrho_g (T - T_0) v) = \frac{\partial}{\partial x}\left(k^* \frac{\partial T}{\partial x}\right) + \frac{\partial}{\partial y}\left(k^* \frac{\partial T}{\partial y}\right). \qquad (15)$$

In the third step, a combination of the continuity equation (5), the momentum equations (7-8) and the state equation (9) is used to write a pressure evolution equation:

$$\frac{\partial (\varepsilon p/T)}{\partial t} = \frac{1}{2}\frac{\partial}{\partial x}\left(\frac{K}{T\mu}\frac{\partial p^2}{\partial x}\right) + \frac{1}{2}\frac{\partial}{\partial y}\left(\frac{K}{T\mu}\frac{\partial p^2}{\partial y}\right) + \frac{W_g}{R}\left(\frac{K}{\mu}\frac{p^2 g}{T^2}\right) + \frac{R\Omega_g}{W_g}. \qquad (16)$$

The equation (16) (initial and boundary conditions reported in Figure (1)) is solved in the place of the total continuity equation (5) to get the pressure distribution, while the momentum equations and the state equation are used to evaluate the velocity components and the gas density, respectively:

$$u = -\frac{K}{\mu}\frac{\partial p}{\partial x}, \quad v = -\frac{K}{\mu}\left(\frac{\partial p}{\partial y} + \varrho_g g\right), \quad p = \frac{\varrho_g R T}{W_g}. \qquad (7-9)$$

Solid densities and porosity evaluated according to eqns (1-3,13) (treated by means of a first-order implicit method) represent the solution advanced

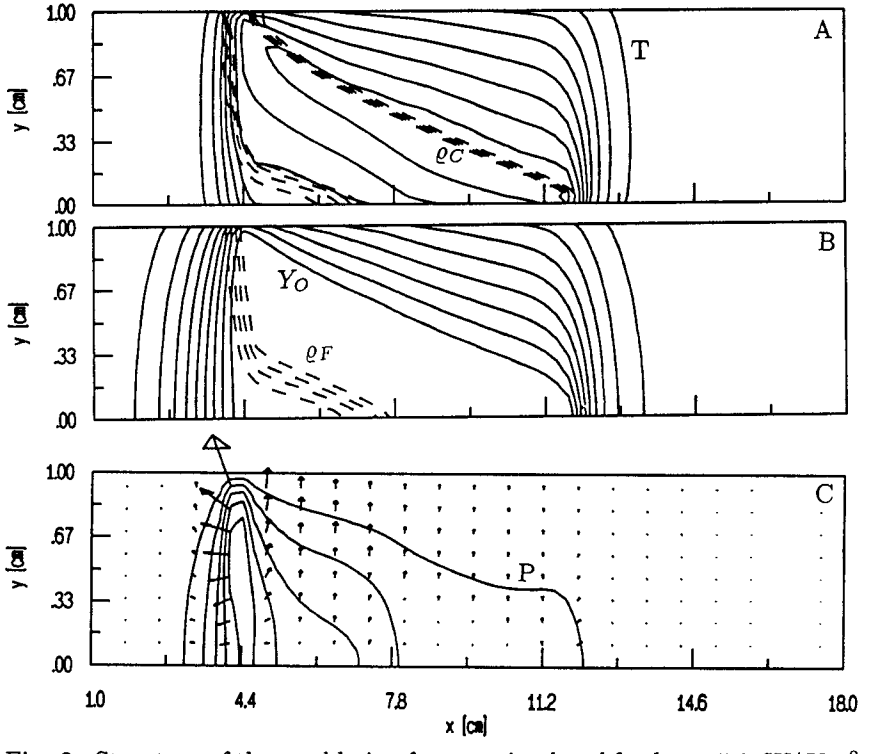

Fig. 2 - Structure of the smoldering front as simulated for $h_w = 5.85 W/Km^2$. A) Contours of temperature [K] (solid lines) from 350 (left) and then increasing with step 50 and char density $[kg/m^3]$ (dashed lines) from 0.75 (right) and increasing with step 0.75. B) Contours of oxygen mass fraction (solid lines) from 0.023 (right) and then increasing with step 0.023 and solid density $[kg/m^3]$ (dashed lines) from 6.8 (right) and increasing with step 6.8. C) Contours of gas overpressure [atm] (solid lines) from 7×10^{-4} (left) and then increasing with step 7×10^{-4} and vector velocity field $[m/s]$ (maximum value 0.025).

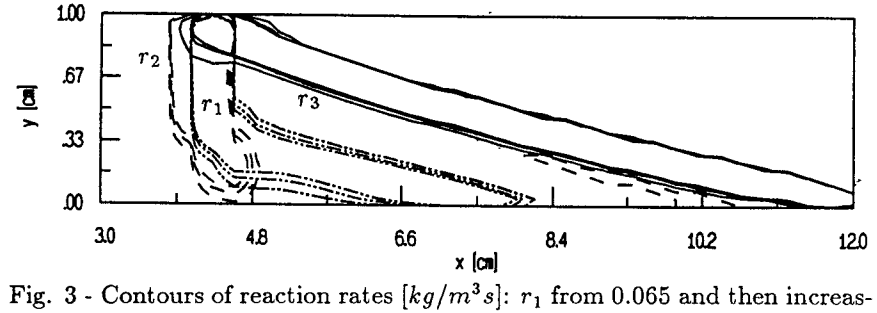

Fig. 3 - Contours of reaction rates $[kg/m^3 s]$: r_1 from 0.065 and then increasing with step 0.065; r_2 from 0.013 and then increasing with step 0.013; r_3 from 0.018 and then increasing with step 0.018.

by the chosen time step, since they are not directly affected by physical processes. On the contrary, temperature and oxygen density distributions are obtained from eqns.(14-15), using the solutions of eqns.(11-12) as starting values. Finally, the highly non linear pressure equation (16) is iteratively solved with the last available values of temperature and volatile production term Ω_g, requiring that, for each time step, the relative differences between two successive pressure values are less than 10^{-3}.

In all cases, the equations describing transport phenomena are approximated with a system of algebraic equations through the hybrid scheme. Also, the two-dimensional spatial operators, describing transport phenomena, are treated by means of a semi-implicit approach based on the ADI method.

A COMPUTATIONAL EXAMPLE

The computer model has been used to simulate the smoldering combustion of a thin ($1cm$) fuel layer ($0.20m$ long) for different values of h_w (downward heat losses). Medium properties describe cellulosic insulation. Apart from the pre-exponential factor of the solid oxidation reaction (c2) estimated as $A_2 = 1.67 \times 10^{13} s^{-1} m^3 kg^{-1}$ and $nF1 = nF2 = nO1 = nO2 = nC1 = 1$, the values of the heat of reaction and the kinetic data for reactions c1) and c2) are taken from [7] while the kinetic data for reaction c3) are those reported in [4]. The convective heat transfer coeffcient is $h_c = 5.85 W/Km^2$ [8] and the mass transfer coefficient is $k_m = 0.5 m/s$ [2]. The time step used for the stages 2) and 3) of the numerical calculations (physical processes) is $2.5 \times 10^{-3} s$. The integration of chemical operators (stage 1)) over the same time step may be accomplished through shorter time intervals on dependence of the convergence requirements. Space and time steps are: $\Delta_x = 0.26cm$ and $\Delta_y = 0.037cm$.

The structure of the smoldering wave can be observed through Figs. 2-3, where temperature, char density, fuel density, oxygen mass fraction, pressure and vector velocity distributions and reaction rate contours are plotted ($h_w = 5.85 W/Km^2$). After the external heat flux is turned off, a self-sustained smoldering front propagates through the solid with a uniform spread rate and, at a first glance, the structure of the front appears to be multi-dimensional. Four main regions can be observed: 1) virgin solid, 2) solid degradation front, 3) charred region and 4) char oxidation front.

For low h_w values ($< 6 W/Km^2$), solid degradation (and subsequent char combustion) occur along the whole thickness of the bed. The solid degradation front is parabolic with a significant decrease in the rate of spread as the bottom surface is approached. As shown by the constant contour levels of reaction rates (Fig.3), at the almost straight part of the solid reaction front, both pyrolytic and oxidative degradation is taking place. On the contrary, in the neighborhood of the bottom surface, degradation is essentially pyrolytic, because oxygen is burned by oxidation of the overhanging solid and char. Also, in this region, temperatures are lower not only because of the downward heat losses, but also because no exothermic reaction occurs. Oxygen

depletion at the solid and char reaction fronts hinders any diffusion across a wide part of the charred region where no reaction occurs. Thus, the highest temperatures are simulated just behind the leading edge of the smoldering front, along the char oxidation front, as a consequence of the significantly large exothermicity of this process.

The flow of gaseous products attains its maximum value in the vicinity of the leading edge of the smoldering front where volatile production is high. Significant gas velocities are also attained along the region where char

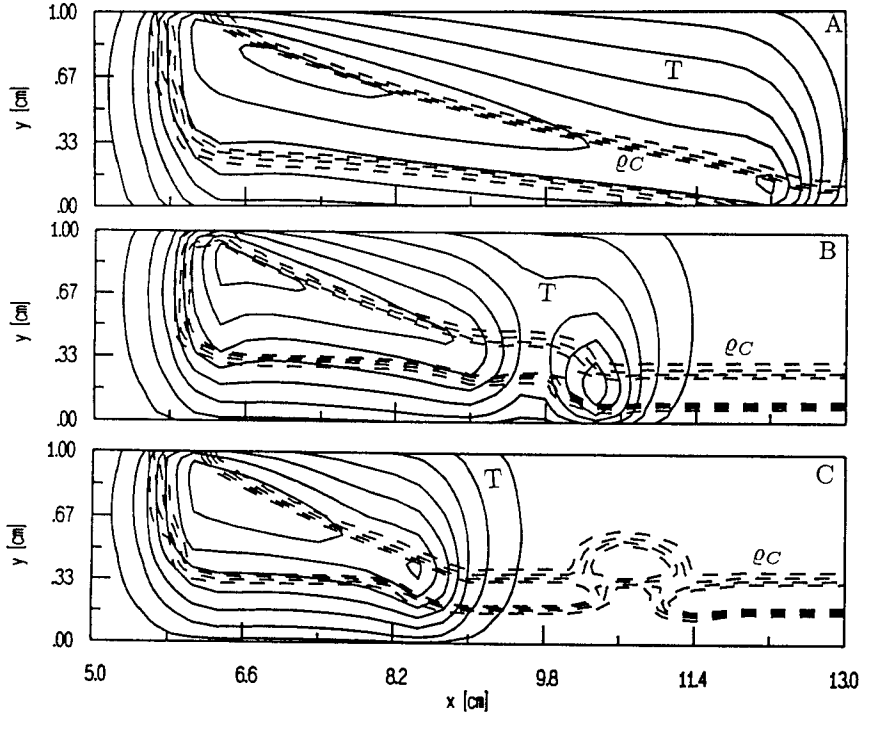

Fig. 4 - Temperature and char density contours as simulated for $h_w = 12.53(A), 29.25(B)$ and $62.7(C) W/Km^2$. Same values as Figure 2.

$h_W[W/Km^2]$ 0.	5.85	12.5	21	62.7
$V_s \times 10^4[m/s]$ 2.6	2.4	2.33	2.26	1.99

Table 1 -Spread rate of the smoldering wave (leading edge) as function of h_w.

oxidation is under way. Pressures sligthly larger than ambient values are simulated at the solid degradation front, where both oxidative and pyrolytic degradation of the solid occurs.

Figures 4A-4C reports temperature and char density contours for three values of h_w larger than that of Figs.2-3. In these conditions, some of the solid, in the vicinity of the bottom surface, is not degraded, because of the reduced temperatures. As expected, the thickness of the unburned solid increases with h_w and solid degradation can also occur at the right boundary of the smoldering wave (high oxygen concentrations and larger temperatures) leading to an irregular shape of the solid left behind the combustion fronts. However, the most evident change observed in the structure of the smoldering wave is associated with successively shorter lengths of the smoldering wave, as h_w is increased. There are two reasons for this finding. In the first place, the char layers become thinner and the time for their complete burn-out shortens. In the second place, as downward heat losses increase and temperatures in the lower part of the bed are reduced, larger gas densities and oxygen diffusive fluxes along the y direction are simulated. Consequently, the larger amount of oxygen, supplied at the left boundary of the smoldering wave, is also responsible for a faster burning of the char. Finally, it should be observed that the rates of spread of the leading edge of the smoldering front only slightly decrease as h_w is increased (Table 1), indicating that the spread process, in the upper part of the bed, is dominated by oxygen diffusion.

REFFERENCES

1) Lai F. C., Prasad V., and Kulacki F. A., Aiding and opposing mixed convection in a vertical porous layer with a finite wall heat source, *Int. J. of Heat and Mass Transfer*, 31, pp. 1049-1061, 1988.

2) Ohlemiller, T. J., Forced smolder propagation and the transition to flaming in cellulosic insulation, *Combustion and Flame*, 81, 354-365, 1990.

3) Ohlemiller, T. J., Smoldering combustion propagation through a permeable horizontal fuel layer, *Combustion and Flame*, 81, pp.341-353, 1990.

4) Ohlemiller, T.J., Bellan, J., and Rogers, F., A model of smoldering combustion applied to flexible polyurethane foams, *Combustion and Flame*, 36, pp.197-215, 1979.

5) Dosanjh S. S., Pagni P. J., and Fernandez-Pello A. C., Forced cocurrent smoldering combustion, *Combustion and Flame* 68, pp. 131-142, 1987.

6) Moallemi M. K., Zhang H., and Kumar S., Numerical modeling of two-dimensional smoldering processes, *Combustion and Flame* 95, pp. 170-182, 1993.

7) Kashiwagi T., and Nambu H., Global kinetic constants for thermal oxidative degradation of a cellulosic paper, *Combustion and Flame* 88, pp. 345-368, 1992.

8) Kinbara T., Endo H., and Sega S., Downward propagation of smoldering combustion through solid materials, *Eleventh Symp. (Int.) on Combustion*, pp. 525-531, 1967.